

Hysteretic behavior of perforated steel plate shear walls with beam-only connected infill plates

Behzad Shekastehband^{*1}, Ali A. Azaraxsh^{1a} and Hossein Showkati^{2b}

¹Department of Civil Engineering, Urmia University of Technology, Urmia, Iran

²Department of Civil Engineering, University of Urmia, Urmia, Iran

(Received June 28, 2017, Revised July 26, 2017, Accepted August 07, 2017)

Abstract. The steel plate shear wall with beam-only connected infill plate (SSW-BO) is an innovative lateral load resisting system consisting of infill plates connected to surrounding beams and separated from the main columns. In this research, the effects of perforation diameter as well as slenderness ratios of infill plates on the hysteresis behavior of SSW-BO systems were studied experimentally. Experimental testing is performed on eight one-sixth scaled one-story SSW-BO specimens with two plate thicknesses and four different circular opening ratios at the center of the panels under fully reversed cyclic quasi-static loading in compliance with the SAC test protocol. Strength, stiffness, ductility and energy absorption were evaluated based on the hysteresis loops. It is found that the systems exhibited stable hysteretic behavior during testing until significant damage in the connection of infill plates to surrounding beams at large drifts. It is also seen that pinching occurred in the hysteresis loops, since the hinge type connections were used as boundaries at four corners of surrounding frames. The strength and initial stiffness degradation of the perforated specimens containing opening ratio of 0.36 compared to the solid one is in the range of 20% to 30% and 40% to 50%, respectively.

Keywords: steel shear wall with beam-only connected infill plate (SSW-BO); analytical method; cyclic loading; hysteresis; dissipated energy

1. Introduction

Steel plate shear walls (SPSWs) as the primary lateral force resisting systems in buildings for high seismic regions have been in use for a long time. Their performance relies on tension field action to provide lateral load resistance (Sabouri-Ghomi *et al.* 2005, Vatansever and Yardimci 2011, Nie *et al.* 2013, Bhowmick *et al.* 2014, Broujerdian *et al.* 2016, Dhar and Bhowmick 2016). Steel plates may be divided into slender, moderate, and stocky categories based on their slenderness ratio as well as buckling and yielding behavior. An unstiffened slender plate buckles elastically at early stages of loading and during its post-buckling path experiences geometrical and material nonlinearities (Zirakian and Zhang 2015).

The use of compact shapes for the columns and ensuring hinges form only near the column bases and near the column tops ensures that the system can achieve collapse prevention performance. Hoseinzadeh Asl and Safarkhani (2017) proposed SPSWs with specific type of reduced beam section. The beam section is weakened with different methods using circular and elliptical web openings, vertical slots in the web and also the reduction of the beam flange.

Previous researches imply that the column demands in SPSWs are complex in nature. Flexural and shear demands result from the horizontal components of tension field action (pull-in forces) and from the frame action. Column axial demands result primarily from resisting the overturning moment resulting from yielding of web plates at stories above. These significant demands on SPSW columns can result in column failures (Berman and Bruneau 2008). Over the last decade, some attempts at mitigating the column demands resulting from pull-in and frame action were addressed by the use of light-gauge, cold-formed steel panels, low yield point steels for the infill plates, reduced beam sections at beam-to-column connections, and strategic placement of holes in the infill panels (Vian and Bruneau 2005, Bruneau *et al.* 2011).

Xue and Lu (1994a,b) suggested reducing pull-in demand on framing adjacent to an SPSW, including the connection of the infill panel to only the beams in a moment frame. Driver *et al.* (2001) also proposed the idea of separating SPSWs from the moment resisting frame resulting in an innovative steel plate shear wall entitled as SSW-BO. In SSW-BO system, the infill plates do not connect to the main columns of the frame. Guo *et al.* (2011) presented a study on the behavior of SSW-BO and observed that the energy dissipation capacity of specimen with stiffeners was larger than that of the specimens without stiffeners. In addition, they showed that both the height-to-thickness ratio and the span-to-height ratio considerably affect the hysteretic behavior of these systems. Jahanpour *et al.* (2011) conducted some tests on SSW-BO systems and showed that these systems have considerable shear strength.

*Corresponding author, Ph.D.,
E-mail: b.shekastehband@uut.ac.ir

^a M.Sc.,
E-mail: aa.azaraxsh@gmail.com

^b Professor,
E-mail: h.showkati@urmia.ac.ir

Clayton *et al.* (2016) investigated the impact of using beam-only-connected web plates on self-centering steel plate shear wall design and seismic performance. Expressions for determining beam demands for purposes of design were developed. Shekastehband *et al.* (2017) performed experimental and numerical study on seismic behavior of low yield strength (LYS) and high yield strength (HYS) SSW-BO systems. They observed that the use of HYS web plates in SSW-BO systems appeared to be a promising solution to strengthen the panels. Wei *et al.* (2017) investigated on a novel partially connected steel plate shear walls. Test results showed that the proposed SPSW exhibited good structural performance in terms of initial stiffness, shear resistance, ductility and energy absorption capability.

In SPSW systems, openings are frequently required in SPSWs for passing utilities, architectural purposes and/or structural reasons. The introduction of circular perforation in the infill plate may assist in alleviating excessive design forces to the surrounding frame members, and therefore, reduce their required size (Bruneau *et al.* 2011). During the last decades, research on the effects of openings on the seismic performance of SPSWs were carried out. Roberts and Sabouri-Ghomi (1992) conducted a series of cyclic quasi-static tests under diagonal loading on thin panels with central circular openings. They proposed an approximation equation for calculating the strength of perforated SPSWs. Pellegrino *et al.* (2009) studied the influence of the dimension, position and shape of one perforation on the linear buckling and the non-linear behavior of steel plates. Purba (2006) proposed a formula to determine the shear strength of a perforated infill plate with the specific perforation pattern proposed by Vian and Bruneau. Valizadeh *et al.* (2012) studied the effects of opening dimensions of plates on the seismic behavior of steel plate shear walls. They observed that the existence of an opening at the center of the panel causes a noticeable decrease in energy absorption of the system. Bhowmick (2014) examined the behavior of unstiffened steel plate shear walls with circular perforations in the infill plates. He suggested an equation for calculation of shear strength reduction of an infill plate with circular perforations.

However, insofar as the authors know, no research has been conducted concerning the effects of both perforation and slenderness of infill plates on the seismic behavior of SSW-BOs. The present study, with regard to the above mentioned interests, is therefore concerned with the problem of seismic behavior of perforated SSW-BOs. The circular perforation herein is considered to be at the center of infill plates. The main objectives of the present work are as follows:

- To determine failure modes and hysteretic behavior of solid and perforated SSW-BOs subjected to cyclic loading;
- To examine the effect of slenderness ratio and perforation ratio of the infill plate on the performance characteristics such as shear strength, stiffness, ductility, and energy dissipation of SSW-BOs;
- To compare analytical and experimental behavior

of SSW-BOs and giving a modification to the analytical equations allowing proper estimation of behavior of the tested specimens.

2. Experimental program

2.1 Specimen preparation

To investigate the effect of opening dimension and slenderness ratio of the infill plate on the seismic behavior of SSW-BOs, eight tests were conducted on the scaled specimens. Experimental models were scaled as 1:6 one-story SSW-BO models, with hinge type connections in boundaries at four corners (Fig. 1). It should be noted that seismic performance of steel shear walls is often studied using small-scale models because of constraints on economics, time, and laboratory space. The test results of small-scale models do not necessarily represent the behavior of full-scale structure. Therefore, in order to employ the model test results to predict the behavior of full-scale structures, the scale effect should be studied. The non-dimensional response of the specimens, e.g., the normalized base shear versus drift index, is scale independent and that fully describes the behavior of a SSW-BO. However, the comparisons between same-scale studied models conducted in the current study do not need scale effect. The slenderness ratio (plate width to thickness ratio) and the opening ratio (opening diagonal to plate height ratio) were considered as variables in these specimens. For this purpose, two thicknesses of 0.8 and 1.25 mm were selected for the plates. For each thickness, a panel without any opening and three panels with circular openings of diameters 100, 150 and 180 mm were tested. Each test is performed under fully reversed cyclic quasi-static loading in the elastic and inelastic response zones of the specimens in compliance with the SAC standard proposed by FEMA350 (2000) test protocol by means of a hydraulic jack of 100 kN capacity. Details of the experimental specimens are shown in Fig. 2. The boundary elements of the frame are similar and consisted of the standard profile double section UNP120. Two 20×30×2 mm box sections were used for stiffening the free edges and preventing more out of plane deformations of infill plates. The horizontal edges of the steel plates were clamped between pairs of a rigid frame beams by the means of two rows of high tensile bolts. Bolts with a diameter of 10 mm were used for connections of infill plate to the surrounding beams. To connect the vertical edges of the steel plates to stiffening boxes, high strength bolts with a diameter of 5 mm were used. The depth and width of the specimens were equal to 620 mm while the depth and width of the infill plates were equal to 500 and 460 mm, respectively. Therefore, the distance between stiffening boxes and main columns is 20 mm. The stiffening boxes did not extend the full height of the infill plate; both ends of the boxes are located intentionally at a distance of 20 mm from the surrounding HBES so as to prevent contact between the stiffening boxes and HBES during deformation of the specimens. Specifications of the experimental specimens are illustrated

Table 1 Specification of specimens

Specimen	Plate thickness t (mm)	Primary columns & beams	Stiffening boxes	Slenderness ratio L/t	Perforation diameter (mm)	Opening ratio t/h
SSW-BO-1	0.8	2UNP120	2 box (20x30x2 mm)	575	0	0
SSW-BO-2	0.8	2UNP120	2 box (20x30x2 mm)	575	100	0.2
SSW-BO-3	0.8	2UNP120	2 box (20x30x2 mm)	575	150	0.3
SSW-BO-4	0.8	2UNP120	2 box (20x30x2 mm)	575	180	0.36
SSW-BO-5	1.25	2UNP120	2 box (20x30x2 mm)	368	0	0
SSW-BO-6	1.25	2UNP120	2 box (20x30x2 mm)	368	100	0.2
SSW-BO-7	1.25	2UNP120	2 box (20x30x2 mm)	368	150	0.3
SSW-BO-8	1.25	2UNP120	2 box (20x30x2 mm)	368	180	0.36

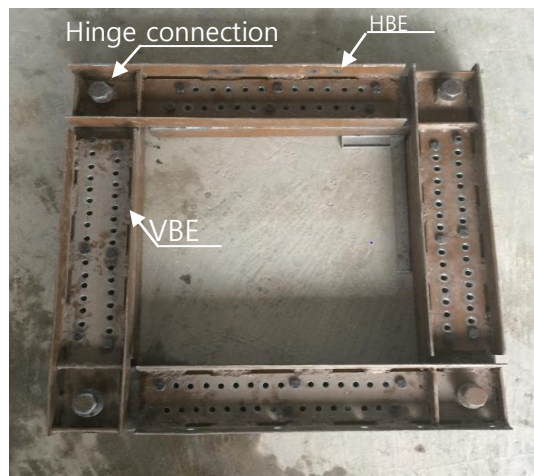


Fig. 1 Hinge type connections in boundaries at four corners

in Table 1.

2.2 Test setup

For each test, after preparing and establishing the specimen on the rigid platform, to prevent out of plane displacement as well as torsional deformation, lateral bracing system including two IPE180 in combination with frictionless rollers were installed at the top level on the both sides of the specimen, as shown in Fig. 3. The applied shear force on the top of upper beam was measured by means of a load cell which was located between hydraulic jack and loading point. To transfer cyclic loads, the hydraulic jack was connected to the top of the specimens through a U-shape pin joint system. Slotted hole on the joint system perpendicular to the line of applied force provides a load path to transfer the force horizontally (Fig. 4).

Four calibrated LVDT (Linear Variable Differential Transformer) transducers were placed on the columns flange to measure the story drift and column deflections. Furthermore, a LVDT transducer was used to monitor the

out of plane displacement of infill plate. For measuring the strains, two single axis strain gauges (St.G0 and St.G1) were installed on the top corners of plate along the diagonals and one single axis strain gauge (St.G2) was located in the vicinity of the circular opening along the secondary diagonal. Locations of the strain gauges were determined at probable plastic zones in the elements based on the preliminary numerical analysis results. A data logger system was used to record the displacements, strains and load at regular intervals during the tests. The position of LVDT transducers and strain gauges is illustrated in Fig. 5.

2.3 Material properties

Tests were conducted to determine the stress–strain curves of the infill steel plates and boundary element materials. Four tensile coupon tests were performed on two infill plate thicknesses to obtain the material properties. The tension test coupon was prepared and tested according to the ASTM A370-05 (2006). The yield stress of steel infill plate with thickness of 0.8 mm and 1.25 mm based on the

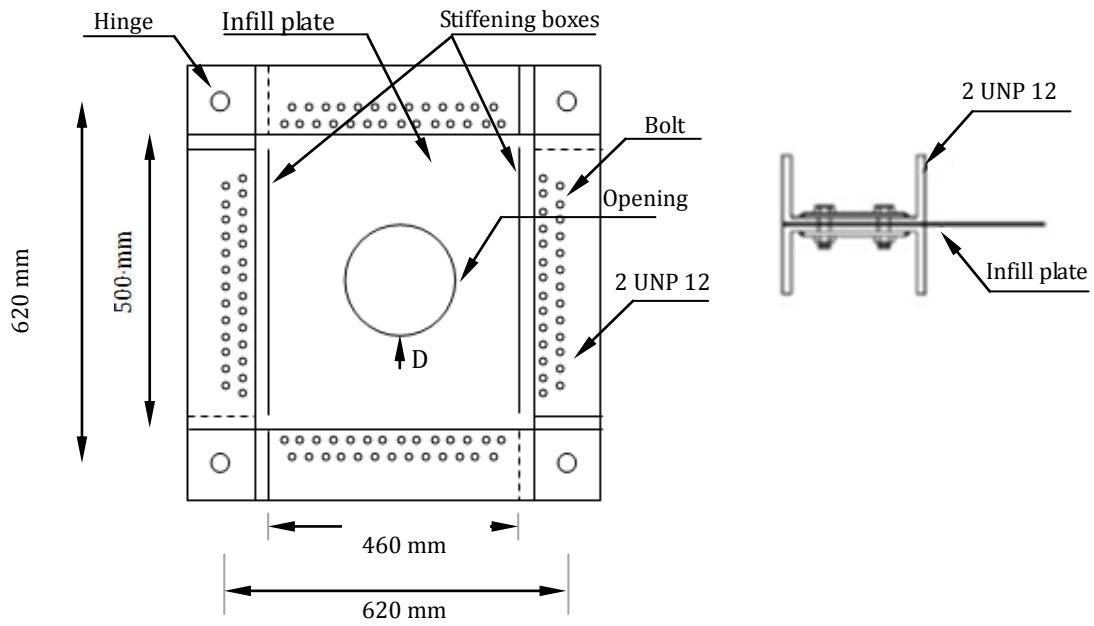


Fig. 2 Details of the experimental specimens

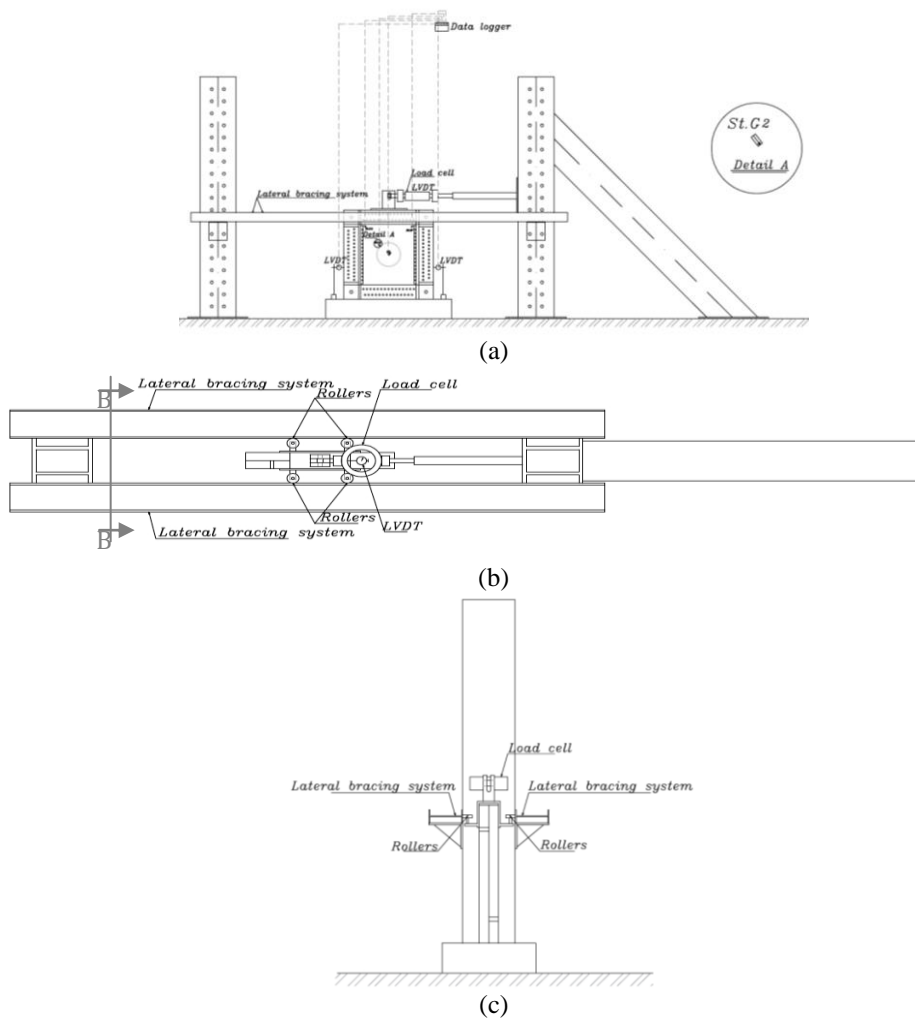


Fig. 3 Schematic view of test set-up of specimens showing the lateral bracing system, rollers, positions of load cell, LVDTs and strain gauges; (a) Front view, (b) Top view and (c) Section B-B

Table 2 Material properties of steel used in the test

Steel material	Elastic modulus (GPa)	Yield stress (MPa)	Yield strain (%)	Ultimate Stress (MPa)	Ultimate strain (%)	Rupture strain (%)
Infill plate (thickness = 0.8 mm)	200	200	0.1	361	18	32
Infill plate (thickness = 1.25 mm)	200	182	0.09	328	27	40
UNP120 & Box 20×30×2 mm	200	240	0.12	360	20	20

mean of coupon tests were found to be 200 MPa and 182 MPa, respectively. Steel material of the surrounding frame and stiffening boxes had yield strength of 240 MPa. The failure strains were approximately at 32%, 40% and 20% for 0.8 mm, 1.25 mm steel infill plate thickness and surrounding members, respectively. A summary of the coupon test results is presented in Table 2.



Fig. 4 Pin connection of hydraulic jack to top of the specimens



Fig. 5 Installation place of the transducers and the strain gauges in the SSW-BO-1 specimen

2.4 Test loading protocol

The quasi-static loading protocol used here was developed based on the guidelines presented in SAC (FEMA350, 2000) and applied horizontally in displacement control to the center of the top beam using an actuator, as shown in the Fig. 3. The loading began with very small values of the overall drift and increased gradually up to a drift of 5%. No vertical load was applied to the specimens. In Fig. 6, the load protocol applied on all the specimens is shown.

3. Experimental results and discussion

3.1 General behavior

Figs. 7(a)-7(h) shows global failure modes of the infill plates in eight specimens. Inspection the connection at the end of testing has shown fracture of the steel plate between adjacent bolts along a row on both solid specimens (Figs. 7(a) and 7(e)). This phenomenon was more pronounced in 0.8 mm thin plate. In addition, local tears appeared adjacent to the corners of infill plates. In specimens with thinner plate, especially for solid and perforated of 100 mm diameter, slippage along connection zone of infill plate to bottom HBE at corners at 3% drift level was accompanied with local tears appeared adjacent to the corners of infill plates at drift value of 4% (Fig. 8). According to the results, in perforated infill plates with thickness of 1.25 mm, there is no noticeable tear on the plate at the corners. As expected, thinner infill plates are more prone to corner fractures. In addition, by either increasing plate thickness or increasing perforation diameter, number of corners contributing in slippage and fracture decreased. Contrary to thinner infill plate, tension field tear was observed for solid specimen with infill plate thickness of 1.25 mm (Fig. 9).

The tear was initiated by low cycle fatigue resulting from the cyclic kinking of the infill plate at the junction of tension fields as the infill plate buckled cyclically with load reversals. Because no plastic deformations were observed in the bolts and stiffening boxes, the steel panels could be dismantled easily after the test.

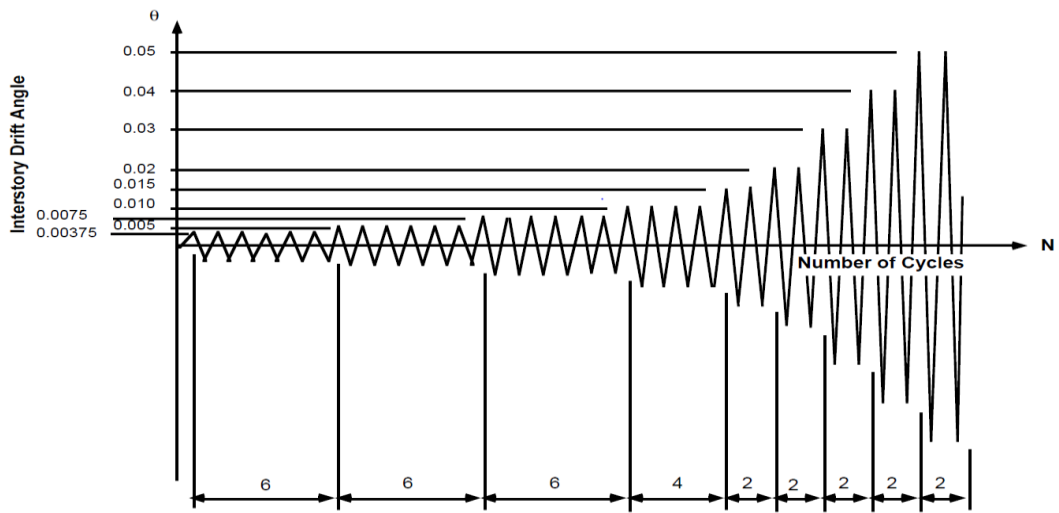


Fig. 6 Loading protocol based on SAC (FEMA, 2000)

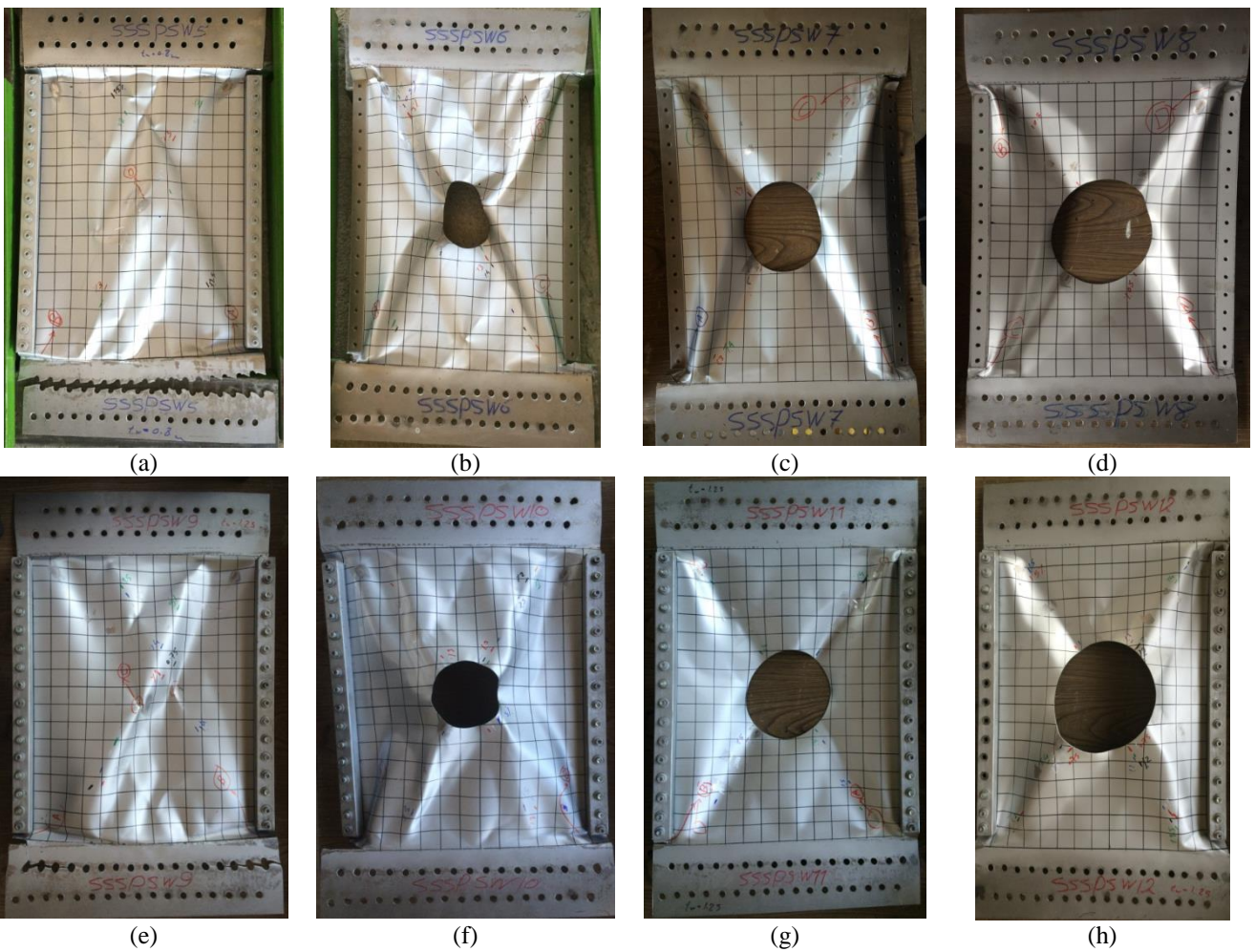


Fig. 7 Failure modes of all the specimens: (a) SSW-BO-1, (b) SSW-BO-2, (c) SSW-BO-3, (d) SSW-BO-4, (e) SSW-BO-5, (f) SSW-BO-6, (g) SSW-BO-7 and (h) SSW-BO-8



Fig. 8 Local tears at the lower corners of SSW-BO-2

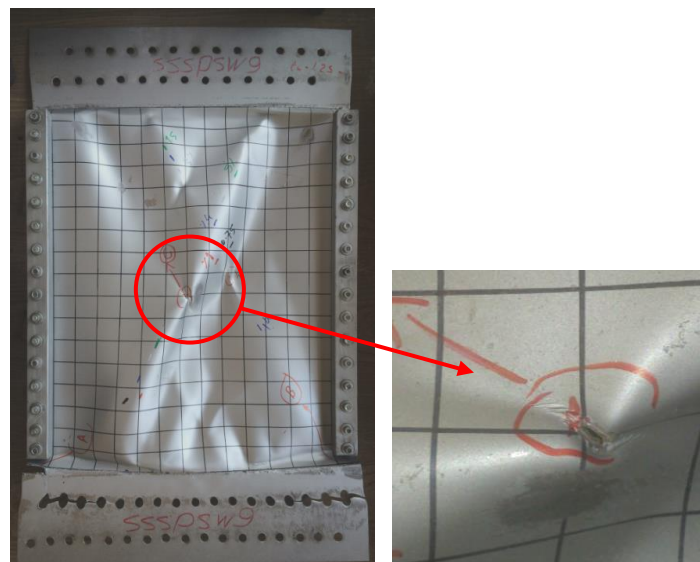


Fig. 9 Tension field tear of specimen SSW-BO-5

This fact, coupled with a small residual drift, allows for the removal of damaged panels after moderate earthquakes. Generally, failure modes of the different specimens can be conclusively classified as:

- Bearing failure in the line of bolts in the solid specimens;
- Local tears at the corners of infill plates in perforated specimens;
- Slippage along connection zone of infill plate in the solid and perforated specimens.
- Complete loading and lack of obvious tears at the corners of perforated panels with thickness of 1.25 mm and perforation ratio in excess of 0.2;

As shown in Fig. 10, out of plane buckling was initiated at the lower corners of steel plate due to its compressive stress state. In fact, the disconnection of stiffening boxes to-HBEs facilitated the out of plane buckling. With the increase of load, the buckling at corners became more

pronounced. In the specimens consisting of infill plates with the thickness of 0.8 mm, formation of tension field line and buckling wave were evident in the last cycles of 0.375% drift level. However, in the infill plates of 1.25 mm thickness, buckling waves could be distinguished in the cycles of around 1% drift. In solid specimens, audible bangs were heard during the positive and negative excursions. For specimens with a perforation diameter of 100 mm (i.e., SSW-BO-2 and SSW-BO-6), the produced bang noise decreased noticeably. However, for two other perforation diameters, namely, 150 mm and 180 mm, there was no sign of bang noise and impact during cyclic loadings. For any plate thickness, by increasing the perforation diameter, the out-of-plane deformation developed dramatically, as shown in Fig. 11.

Average inclination angle of tension fields for all the specimens through measuring the inclination of the buckled waves are presented in Table 3. For any thickness of infill plates, as illustrated in Table 3, there was an increase in the



Fig. 10 Out of plane buckling at the lower corners at early stage of loading: (a) SSW-BO-5 and (b) SSW-BO-7



Fig. 11 Out of plane deformation at 3% drift: (a) SSW-BO-1, (b) SSW-BO-2, (c) SSW-BO-3 and (d) SSW-BO-4

Table 3 Measured tension field inclination of the specimens

Specimen	SSW-BO-1	SSW-BO-2	SSW-BO-3	SSW-BO-4	SSW-BO-5	SSW-BO-6	SSW-BO-7	SSW-BO-8
Inclination Angle	29	30	33	33	29	30	33	35

Table 4 Measured load of the specimens during the test

Specimen	Measured load (kN)									Strength degradation (%)
	0.375	0.5	0.75	1	1.5	2	3	4	5	
SSW-BO-1	10.99	14.43	17.386	18.86	20.58	19.60	20.34	18.37	15.91	22.71
SSW-BO-2	9.76	12.71	16.40	16.89	18.12	18.37	20.34	22.30	21.07	5.51
SSW-BO-3	9.27	10.50	12.71	12.96	14.43	15.17	17.14	18.37	17.38	5.36
SSW-BO-4	7.38	9.27	11.97	12.71	14.43	14.68	15.91	16.15	16.15	0.00
SSW-BO-5	12.71	15.91	22.80	26.90	28.62	29.60	31.08	31.32	25.01	8.64
SSW-BO-6	7.63	11.97	19.60	23.29	25.75	25.75	26.65	27.88	28.37	0.00
SSW-BO-7	8.61	10.00	17.88	19.35	21.81	22.30	24.27	25.01	25.26	0.00
SSW-BO-8	10.74	12.46	15.66	17.38	19.35	19.60	21.07	21.81	22.55	0.00

inclination angle of the SSW-BOs as the perforation diameter increased. It was observed that inclination angles of SSW-BOs were lesser than the recommended values between 38° and 50° for SPSWs (Bruneau *et al.* 2011). Despite the change in buckling wave directions, the out-of-plane buckling direction remained unchanged. Development of second buckling waves along the same direction as the main wave was initiated at drift values more than 1%. However, when the perforation diameter was increased, second waves were not appreciable.

3.2 Hysteretic behavior

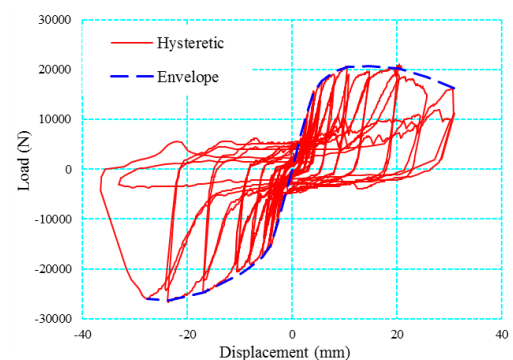
The hysteresis plots of lateral strength versus story displacement along with envelope curves for all specimens are shown in Figs. 12(a)-12(h). In general, the hysteretic loops exhibit pinching in the hysteretic curves, stable ductile behavior. The hysteresis envelope curves of the specimens are presented in Fig. 13.

In the early stages of loading up to around 0.5% drift, the panels behave in a stiff manner. However, as the deformation increased, portions of the steel infill plates yielded, resulting in a gradual decrease of the stiffness. In all the specimens, when the drift ratio reached around 1.0%, the rigidity decreased evidently. At this point, the pinching effect of hysteretic curves appeared due to the accumulated diagonal plastic stretch of the infill plate as the drift cycles increase. The pinching of the hysteretic curves, is more pronounced as the drift ratio increases, and by itself, is not detrimental to the seismic behavior of the systems (Purba and Bruneau 2015). Nonlinear behavior of the specimens was observed at drift levels around 1% where the widening of hysteretic loops was noticed. The use of low yield steel infill plates caused the plates to be nonlinear at lower shear.

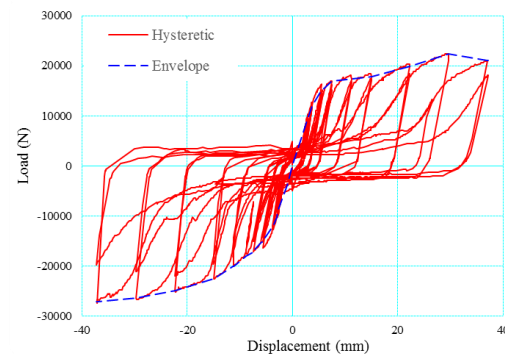
From comparison of the shape of loops corresponding to same drift, it was found that the tolerated load was greater in first cycle and was slightly lower in next loops because of residual strains and plastic deformations caused by first cycle.

In SSW-BO-1, SSW-BO-2 and SSW-BO-3, there is a relative difference between the load-displacement hysteretic curves of the positive and negative regions during load

reversal. For these specimens, an ultimate shear strength of 21.074 kN (-26.65 kN), 22.304 kN (-27.388 kN) and 18.368 kN (-25.502 kN) was reached with the corresponding drift ratio of 3% (-3%), 4% (-5%) and 4% (-4%), respectively. The specimens behaved symmetrically during load reversal until one of the VBEs came in contact with the platform especially at the larger drifts which cause an increase in the shear strength. This effect was more pronounced for solid SSW-BO-1 specimen. Unlike the other specimens, SSW-BO-1 was loaded up to 4% drift and due to plate fracture, the test was terminated at this point. However, the problem was alleviated in the next specimens.

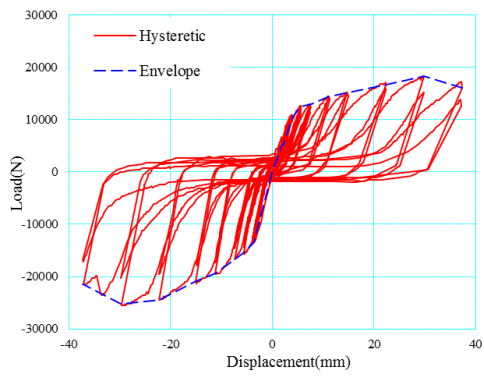


(a)

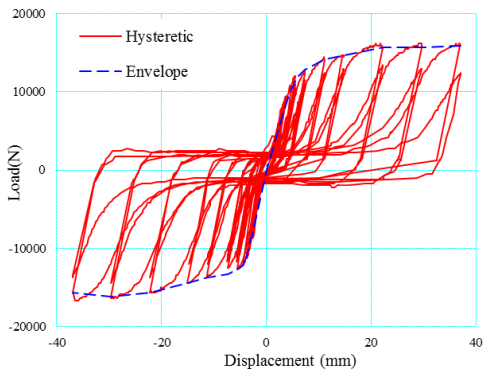


(b)

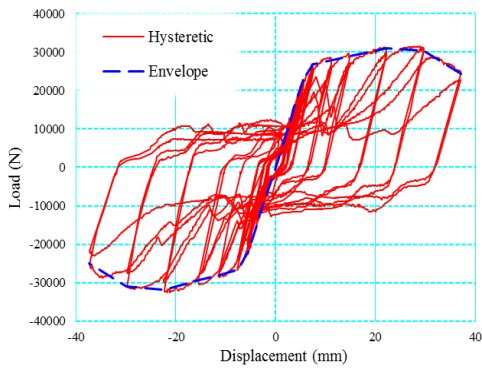
Continued-



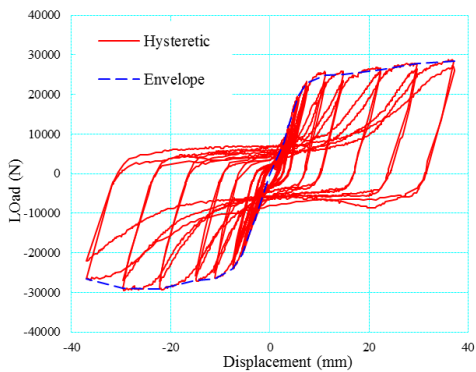
(c)



(d)

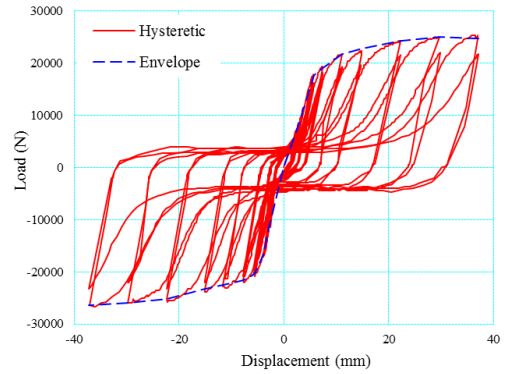


(e)

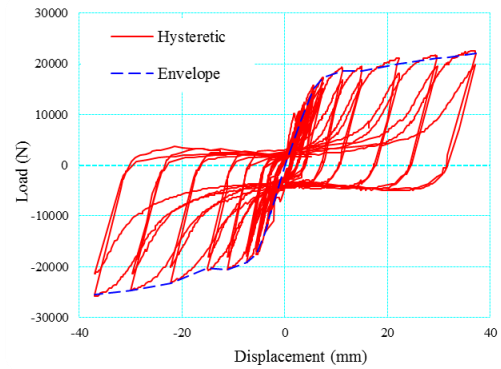


(f)

Continued-



(g)



(h)

Fig. 12 Force-displacement hysteretic curve of the specimens: (a) SSW-BO-1, (b) SSW-BO-2, (c) SSW-BO-3, (d) SSW-BO-4, (e) SSW-BO-5, (f) SSW-BO-6, (g) SSW-BO-7 and (h) SSW-BO-8

Table 4 lists the measured positive loads at drift levels for each of the test specimens. As illustrated in Fig. 13 and Table 4, at the end of the loading program, the shear strength decreased by 22.71% and 8.64% in SSW-BO-1 and SSW-BO-5, respectively.

In the perforated specimens, after pushing the drift over the crest, the degradation in the shear strength of the perforated specimens is slightly (less than 6%) for the thinner infill plate (0.8 mm).

This issue is largely due to the reduced panel strength putting lower demand on the connections to the beams. Furthermore, the results revealed that ultimate capacity is a function both of infill plate thickness and perforation diameter. Specimens with less thickness and higher perforation diameters possess lower ultimate capacity. The strength degradation of solid specimens SSW-BO-1 and SSW-BO-5 can be attributed to major plate connection fractures at drifts in excess of 3%. It is worthwhile to emphasize that in perforated specimens, small tears developed at drifts around 4% had no significant impact on behavior or loss in ultimate capacity.

3.3 Dissipated energy

Dissipated hysteretic energy is an important characteristic affecting the seismic performance of the SPSWs. The area of hysteretic curve denotes the absorbed

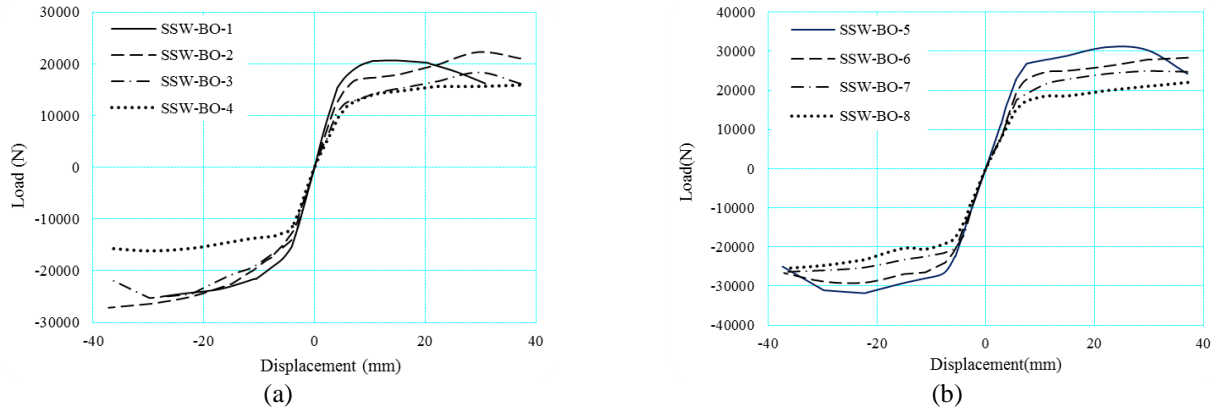


Fig. 13 The hysteresis envelope curves: (a) For specimens with infill plate of 0.8 mm thickness and (b) For specimens with infill plate of 1.25 mm thickness

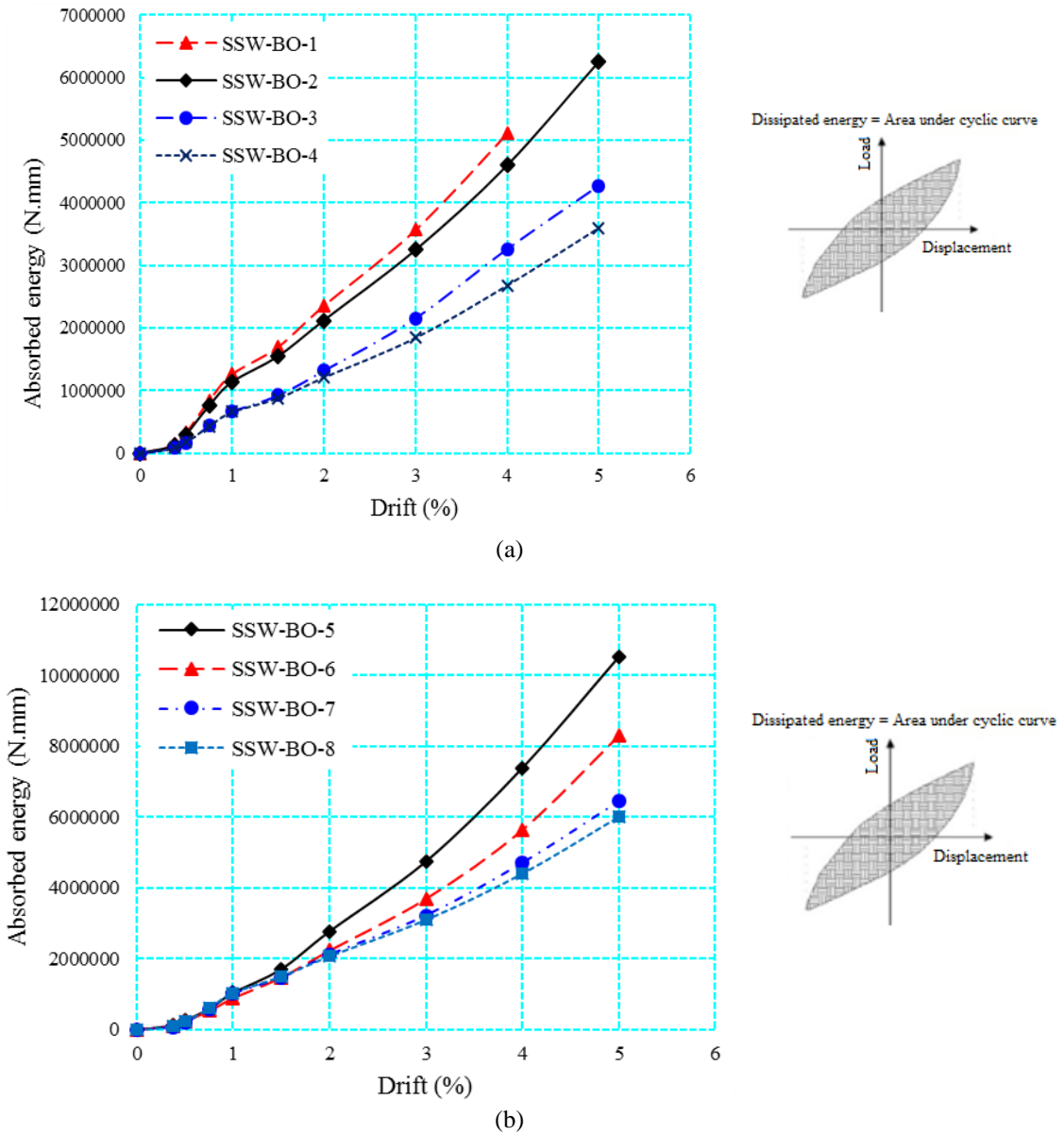


Fig. 14 The relationship curve of area of hysteretic curves versus story drift: (a) For specimens with infill plate of 0.8 mm thickness and (b) For specimens with infill plate of 1.25 mm thickness

Table 5 Cumulative dissipated energy at the 4% drift and ductility of the specimens

Specimen	SSW-BO-1	SSW-BO-2	SSW-BO-3	SSW-BO-4	SSW-BO-5	SSW-BO-6	SSW-BO-7	SSW-BO-8
Dissipated Energy, E (KJ)	5.15	4.60	3.26	2.68	7.39	5.65	4.71	4.41
E. rel.* (KJ/KJ)	1.00	0.89	0.63	0.52	1.00	0.76	0.64	0.60
Ductility $\mu = \Delta_u / \Delta_y$	7.8	7.4	7.16	6.7	6.7	6	5.9	5.78

* Calculated as ratio of energy over solid one for each infill plate thickness

energy in each loading step experienced by the specimen during the test. A comparison of cumulative dissipated energies versus drift of all the specimens is shown in Fig. 14. Table 5 lists the values of cumulative dissipated energy at the 4% drift. In the specimens, with increasing drift, cumulative dissipated energy of the specimens increased.

The dissipated energies do not differ very much at drifts of around 0.5% because the response is almost entirely elastic. From comparison of the results, it is found that for any infill plate thickness, the dissipated energies by solid specimen was more than the perforated ones at the all phases of the testing. It can be seen that with an increase in the perforation diameter, hysteretic pinching increases, leading to reduction of dissipated energy. The cumulative dissipated energy of the SSW-BO-2, SSW-BO-3 and SSW-BO-4 specimens, at the 4% drift, compared with SSW-BO-1 decreased by 11%, 37%, and 48%, respectively. Likewise, reduction in the dissipation capacity of the SSW-BO-6, SSW-BO-7 and SSW-BO-8 specimens, compared with SSW-BO-5 was 24%, 34% and 40%, respectively. In addition, increasing the thickness of the infill plates from 0.8 mm to 1.25 mm resulted in a substantial increase of the energy dissipation capacity of the system.

A 79%, 23%, 44% and 65% enhancement in the absorbed energy of SSW-BO-5/SSW-BO-1, SSW-BO-6/SSW-BO-2, SSW-BO-7/SSW-BO-3 and SSW-BO-8/SSW-BO-4, respectively at drift of 4% was observed. As it can be observed, the high absorption capacity of the SSW-BO-5 and SSW-BO-6 in comparison with the other specimens implies their suitable seismic behavior. Moreover, the amount of the absorbed energy in the SSW-BO-2 and SSW-BO-8 specimens is appropriately close indicating combined effects of perforation diameter and plate thickness on the energy dissipation capacity.

3.4 Ductility evaluation

The test results showed the specimens exhibited very stable behavior until the end of the loading program with a story drift angle of 5%. One goal of the experimental program was to evaluate the ductility. The ductility can be defined as

$$\mu = \frac{\Delta_u}{\Delta_y} \quad (1)$$

where μ is the displacement ductility factor, Δ_u the ultimate displacement and Δ_y the yield displacement.

It is interesting to note that Δ_y has no standardized definition. In these systems with slender steel infill plates, detection of the first yielding is cumbersome due to the nonlinear elastic behavior of the plates. For evaluating the yield displacement Δ_y (Fig. 15), a method recommended in ECCS (1985) was adopted which is based on the tangent of the 10% slope of the initial stiffness. The ultimate displacement Δ_u is the maximum displacement obtained during testing. Ductility factors of all the specimens are provided in Table 5. It can be observed that ductility factor decreases with increasing the perforation diameter of infill plate. In addition, there is a reduction in the ductility factor of the SSW-BOs as the infill plate thickness increases.

3.5 Secant stiffness

In the early stage of loading, all the specimens behaved in an elastic manner. However, it is the commencement of infill plate yielding that generally results in a decrease in the secant stiffness. A comparison of specific stiffness versus drift ratio of the specimens was calculated using secant method and illustrated in Fig. 16. Secant stiffness decreased in the specimens along with increasing overall drifts. However, stiffness degradation was more intensive at the early stage of loadings especially for solid specimens. Clearly, the higher the perforation diameter, the lower is secant stiffness. Moreover, increasing the thickness of the infill plate increased the secant stiffness of the specimens.

At the drift of 1.5%, secant stiffness of the SSW-BO-2, SSW-BO-3 and SSW-BO-4 specimens decreased by 2%, 22% and 32%, respectively, with respect to SSW-BO-1 specimen. A similar conclusion was drawn for the other specimens associated with infill plate of 1.25 mm thickness.

The discrepancy between secant stiffness of the solid and perforated specimens decreased at larger drifts (greater than 3%).

Table 6 Comparison of the experimental and theoretical results of the specimens

Specimen	Experimental			Theoretical	
	Initial stiffness (kN/mm)	Ultimate P_u^+ (kN)	Strength P_u^- (kN)	Initial stiffness* (kN/mm)	Shear strength** (kN)
SSW-BO-1	4.41	21.074	26.650	3.42	20.28
SSW-BO-2	3.22	22.304	27.388	2.74	16.22
SSW-BO-3	2.50	18.368	25.502	2.40	14.19
SSW-BO-4	2.33	16.154	16.646	2.19	12.98
SSW-BO-5	4.69	31.570	32.555	5.35	28.83
SSW-BO-6	3.73	28.864	29.602	4.28	23.07
SSW-BO-7	3.24	25.256	26.650	3.74	20.18
SSW-BO-8	2.72	22.550	25.748	3.42	18.45

* Calculated using Eq. (5)

** Calculated using Eq. (4)

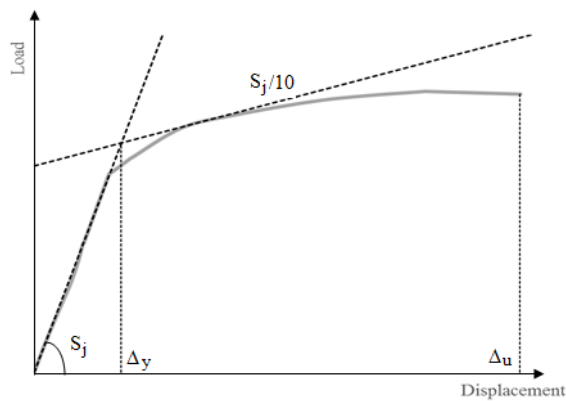


Fig. 15 Determination of yielding displacement Δ_y

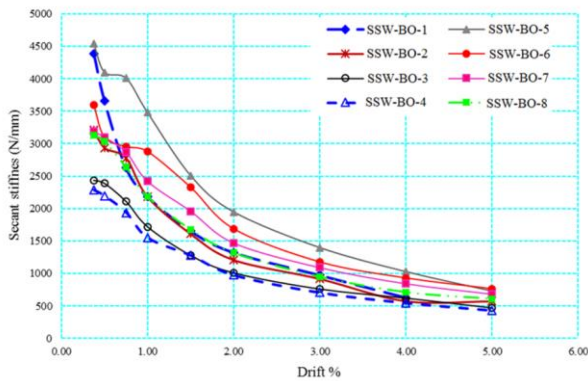


Fig. 16 Comparison of secant stiffness

3.6 Strain results

Specimen SSW-BO-6 and SSW-BO-7 are taken for an example to illustrate the recorded strains. Recorded strains during cyclic testing are presented in Figs. 17(a) and 17(b) for SSW-BO-6 and SSW-BO-7, respectively. The envelope strain (corresponding to the maximum target drift of every cycle) progressively increased from practically zero in the

first displacement step to 0.056, 0.054, 0.04 and 0.076 respectively for St.G1-SSW-BO-6, St.G2-SSW-BO-6, St.G1-SSW-BO-7 and St.G2-SSW-BO-7 when the specimens were cycled up to 5% drift amplitude. There is a reduction in the strains of corners (St.G1) of infill plates as the perforation diameter increases. The magnitude of strain (St.G2) in the vicinity of circular opening increases with increasing perforation diameter. The results are consistent with the failure modes observed in the specimens. As the perforation ratio increased, the strains developed at the corners became relatively small, and therefore, progression of tears was ceased. Moreover, growth of out of plane deformation as a function of perforation ratio causes an increase of the strains in vicinity of the perforation. The same trend was also observed on the progression of the residual strain when the structure returned to its original position at 0% drift. The accumulation of plastic incremental strain predominantly occurred in the displacement greater than 7 mm (1.0% drift).

3.7 Stiffness and shear strength

The initial lateral stiffness and ultimate shear strength of all the specimens based on the test results is given in Table 6. As expected, increasing perforation ratio of infill plate up to 0.36 resulted in a reduction of both initial stiffness and shear strength up to roughly 45% and 25%, respectively.

This can be explained by the fact that the infill plate area decreases with the increase of opening ratio and therefore, the contribution of the infill plate tension field action to the overall behavior decreases, with this effect, the stiffness, ductility and strength of the perforated SSW-BOs decreases with the opening ratio. As seen in Table. 6, initial stiffness and strength of the specimens tend to decrease as much as roughly 14% and 28%, respectively as the slenderness ratio of the infill plates increases from $H/t = 400$ to 625. This issue is also attributed mainly as a consequence of the less tension field action provided by the slender infill plates.

The results can be compared to theoretical shear force V -horizontal displacement Δ skeleton curve. It is assumed that the theoretical skeleton curve is elastic-perfectly plastic as shown in Fig. 18.

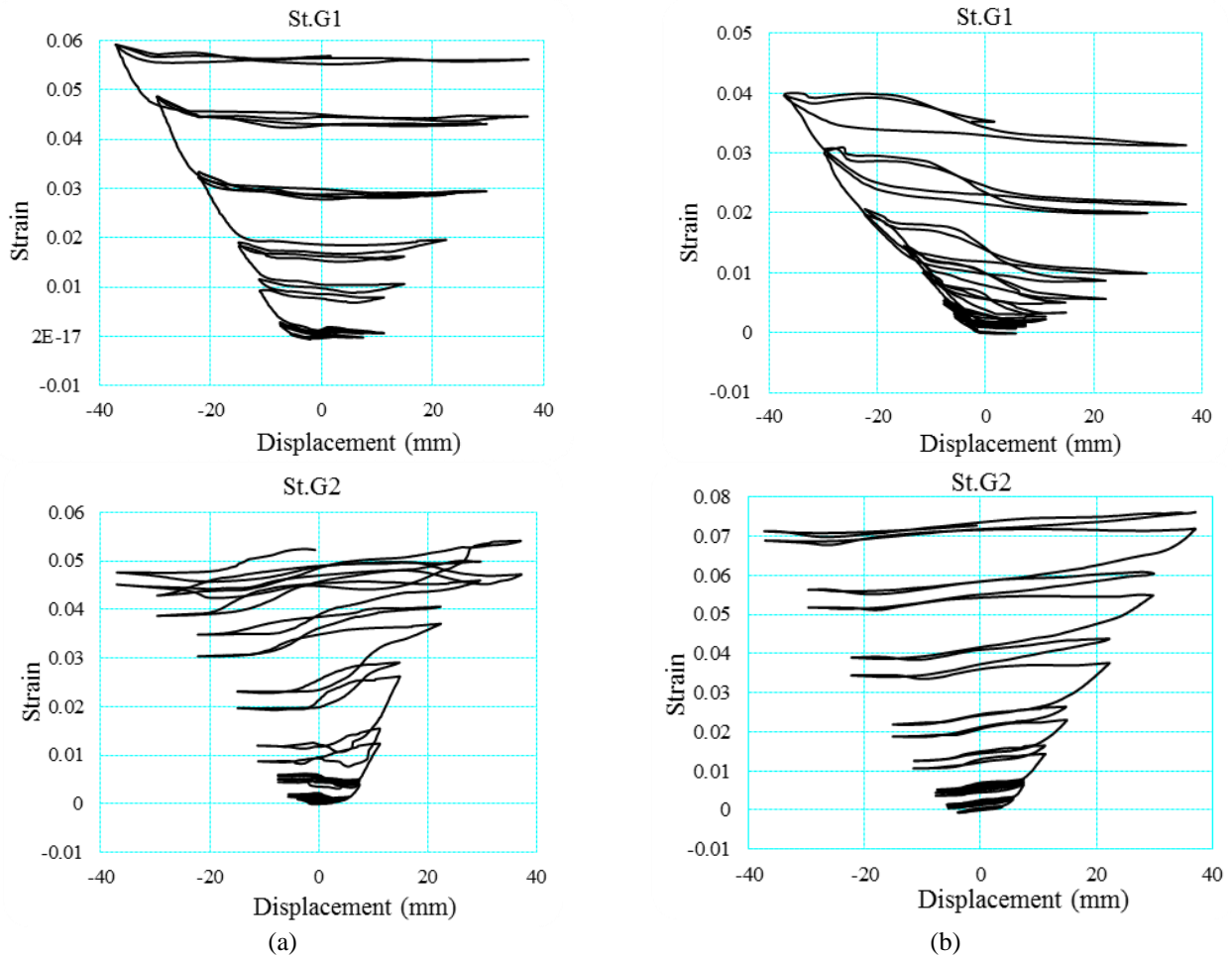


Fig. 17 Strains versus lateral displacement: (a) SSW-BO-6, (b) SSW-BO-7

The surrounding frame provides no considerable contribution to lateral load resisting. Therefore, the shear strength of specimens is mainly supplied by infill plate. As shown in Fig. 19, the SSW-BO can be idealized as a member fixed at both ends, for which the frame beams act as the fixed ends (Guo *et al.*, 2011).

Considering both the shear and bending deformations of the infill plate, the theoretical initial stiffness proportional to the lateral displacement is obtained as (Guo *et al.* 2011)

$$K_0 = \frac{Et}{1/(L/H)^3 + 2(1+\nu)k/(L/H)} \quad (2)$$

where, L , H , t and k are the length, height, thickness and correction coefficient equal to 1.2, respectively.

It is noteworthy that shear strength of infill plates in SSW-BOs is somewhat different from counterparts in SPSWs. The columns do not contribute to restraining the infill plate in the specimens. Therefore, a partial tension field over the diagonal of the plate restrained by both surrounding beams is developed (Fig. 20). The nominal lateral strength of the infill plates in these specimens can be determined based on the equation of lateral strength of infill plates in SPSWs presented in AISC seismic provisions by

inclusion some modifications (Clayton *et al.* 2015)

$$V_n = 0.42F_y t L_{PTF} \sin 2\theta \quad (3)$$

where $L_{PTF} = L - H \tan(\theta)$ is the length of partial tension field along the beams, and $\theta = 0.5 \arctan(L/H)$ is the partial tension field angle of inclination (Clayton *et al.* 2015).

However, considering the cyclic strain-hardening effect and probable steel yield strength, the authors proposed that the probable maximum lateral strength (V_{pr}) of infill plate to be calculated as

$$V_{pr} = 0.5C_{pr}R_yF_y t L_{PTF} \sin 2\theta \quad (4)$$

where C_{pr} is the factor to account for the cyclic strain-hardening effect and R_y is the yield stress adjustment factor. These factors are assumed to be $C_{pr} = 1.1$ and $R_y = 1.3$ in AISC 341 (2010).

Generally, in the steel plate shear walls with a bolted connection between infill plate and boundary elements, slippage at the bolted connection initiates yielding adjacent to the boundaries and decreases the wall stiffness (Elgaaly 1998).

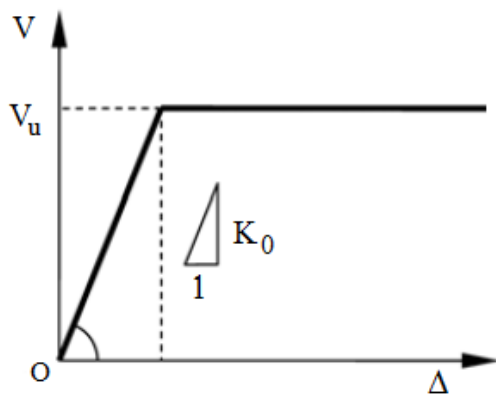


Fig. 18 Simplified model of shear force-displacement Skeleton curve of a steel plate (Gue *et al.* 2011)

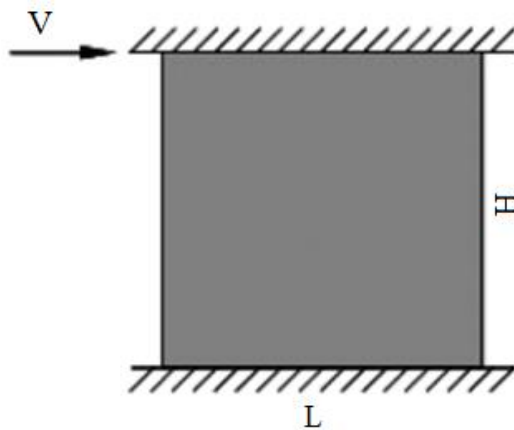


Fig. 19 Steel plate connected to frame beams only (Gue *et al.* 2011)

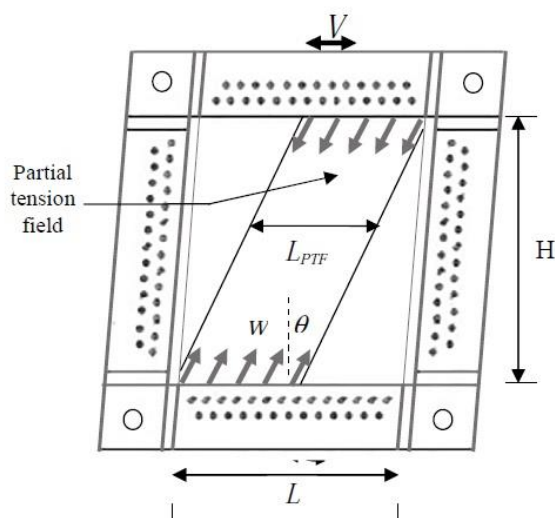


Fig. 20 Steel plate connected to frame beams only

Therefore, by anticipating bolt slippage and geometrical imperfections of the experimental specimens, the stiffness of the specimens was taken as

$$K_{eff} = K_0/n \tag{5}$$

Here, the value of $n = 10.0$ is considered based on the measured stiffness of the specimens. The reduction factor $(1-D/H)$, where D is the opening diameter and H is the panel height, proposed by Roberts and Sabouri (1992) was used in the aforementioned formulas for considering the strength and stiffness decrease in perforated specimens in the present study.

The initial stiffness and ultimate shear strength calculated using theoretical formulations (Eqs. (4) and (5)) were also given in Table 6. Specimens SSW-BO-1, SSW-BO-4, SSW-BO-5 and SSW-BO-8 were taken for example to illustrate the comparison of the theoretical elastic-perfectly plastic curves and the envelope of the test hysteresis curves (Fig. 21). The shear strength and stiffness of “Last Theoretical” curve was obtained using Eqs. 2 and 3, respectively. As can be seen in Table 6 and Fig. 21, the analytical stiffness (Eq. (2)) was overestimated which can be attributed to slippage in bolted connections. The Eq. (3) estimated the nominal shear strength of the experimental specimens more conservatively. However, in “Modified Theoretical” curve, the strain-hardened strength of infill plate and expected yield strength was taken into account (Eq. (4)) and initial stiffness was obtained using Eq. (5). As illustrated in Fig. 21 and Table 6, because the resulting difference between modified analytical method and experimental ones is rather small, therefore, Eqs. (4) and (5) are proved to provide a satisfactory conservative estimate of stiffness and strength of the specimens.

4. Conclusions

In this research, the seismic behavior of the steel plate shear walls with beam-only connected infill plates was experimentally investigated. Eight 1:6-scale specimens were designed and tested under cyclic loading to evaluate the effect of the perforation diameter and the thickness of infill plate on the stiffness, shear strength, cumulative dissipated energy and other important seismic parameters in these systems. Based on the obtained results, the following observations and conclusions were drawn. Strictly speaking, the scope of the conclusions is limited to the conditions considered for the specimens. However, it is likely that the conclusions are of more general applicability.

- In general, energy absorption of the specimens with plate thickness of 0.8 mm is about 70% (on average) of the counterparts with plate thickness of 1.25 mm. By increasing the perforation ratio up to 0.36, cumulative dissipated energy decreased more than 40% with respect to the solid ones;
- The solid specimens failed by plate to beams connection bearing action leading to strength degradation by as much as 23% and 9% in panels with 0.8 mm and 1.25 mm thickness, respectively.

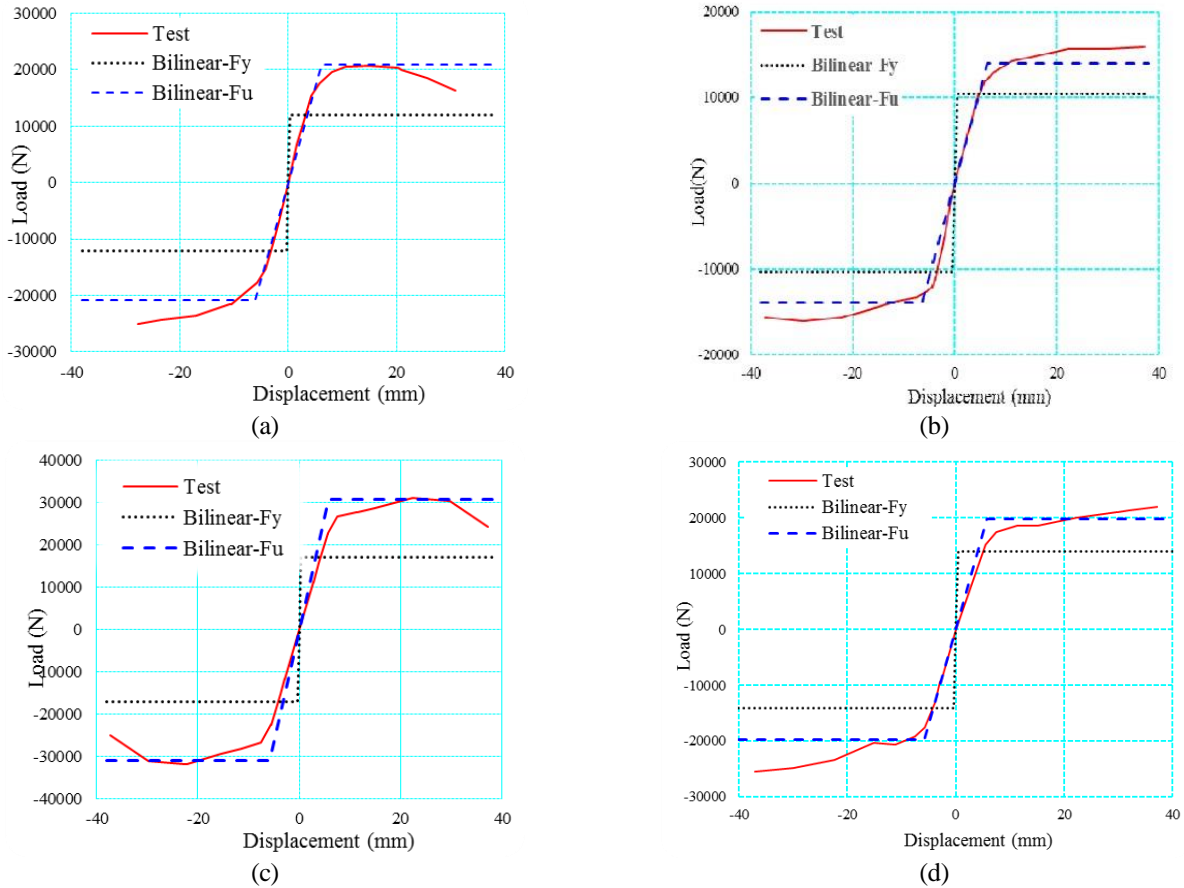


Fig. 21 Comparison of experimental skeleton and theoretical bilinear curves: (a) SSW-BO-1, (b) SSW-BO-4, (c) SSW-BO-5 and (d) SSW-BO-8

Perforated specimens exhibited tearing-tilting failure at the corners mostly for plates with less thickness. The tear was initiated by low cycle fatigue resulting from the cyclic kinking of the infill plate at the corners as the infill plate buckled cyclically with load reversals. In the perforated specimens with infill plate thickness of 1.25 mm, significant tears affecting shear strength were not observed during the test. However, slight degradation of shear strength in the perforated specimens with infill plate thickness of 0.8 mm was caused by an increase in the number of tears and growth of the existing tears;

- For a selected circular perforation with a maximum opening ratio of 0.36, the ratio of perforated specimen strength to the solid one was about 77% and 71% for panels with plate thickness of 0.8 mm and 1.25 mm, respectively. The initial stiffness loss of the perforated specimens compared to the solid one was as much as 47% and 41% for panels with 0.8 mm and 1.25 mm thickness, respectively;
- An increase in the width-thickness ratio leads to both strength and stiffness degradation, which can cause significant reduction up to 23% (by

comparing SSW-BO-3 and SSW-BO-7) and 32% (by comparing SSW-BO-1 and SSW-BO-5) in stiffness and strength, respectively;

- It was derived that the ductility factor (μ) of the solid specimens with infill plate thickness of 0.8 mm and 1.25 mm is $\mu = 7.8$ and 6.7, respectively, that is greater than the perforated counterparts values;
- The average angle of inclination of the tension field measured during the test was between 28° and 35° depending on the perforation diameter. There was an increase in the tension field inclination as the opening ratio increased;
- Contrary to the theoretical model containing perfect geometry and ideal connections, the experimental specimens experienced low initial stiffness due to developing slippage along the bolt connections of infill plate to surrounding beams and presence of initial imperfections;
- The ultimate shear strength of the experimental specimens using theoretical model was estimated conservatively. However, a modification made to the theoretical method allowed proper computation of the stiffness and ultimate strength of the experimental specimens.

Acknowledgments

Thanks Mr. A. Pavir for his helpful contribution to this work.

References

- AISC (2010), "Seismic Provisions for Structural Steel Buildings", ANSI/AISC 341, Chicago: AISC.
- ASTM (2006), "American Society for Testing and Materials Standard test methods and definitions for mechanical testing of steel products", ASTM A370, West Conshohocken, USA.
- Berman, J.W. and Bruneau, M. (2008), "Capacity design of vertical boundary elements in steel plate shear walls", *AISC EJ*, 57-71.
- Bhowmick, A.K. (2014), "Seismic behavior of steel plate shear walls with centrally placed circular perforations", *Thin Wall. Struct.*, **75**, 30-42.
- Bhowmick, A.K., Gilbert, Y., Grondin, G.Y. and Driver, R.G. (2014), "Nonlinear seismic analysis of perforated steel plate shear walls", *J. Constr. Steel Res.*, **94**, 103-113.
- Broujerdian, V., Ghamari, A. and Ghadami, A. (2016), "An investigation into crack and its growth on the seismic behavior of steel shear walls", *Thin Wall. Struct.*, **101**, 205-212.
- Bruneau, M., Uang, C.M. and Sabelli, R. (2011), *Ductile design of steel structures*, Mc Graw Hill (Second Edition).
- Clayton, P.M., Berman, J.W. and Lowes, L.N. (2015), "Seismic performance of self-centering steel plate shear walls with beam-only-connected web plates", *J. Constr. Steel Res.*, **106**, 198-208.
- Dhar, M.M. and Bhowmick, A.K. (2016), "Seismic response estimation of steel plate shear walls using nonlinear static methods", *Steel Compos. Struct.*, **20**(4), 777-799.
- Driver, R.G., Grondin, G.Y., Behbahanifard, M., Hussain, M.A., (2001), "Recent developments and future directions in steel plate shear wall research", *Proceedings of the North American steel construction conference.*, May, Ft. Lauderdale, FL, USA.
- ECCS (1985), "Recommended testing procedures for assessing the behavior of structural elements under cyclic loads", *European convention for constructional steelwork*. Technical Committee 1, TWG 1.3 – Seismic Design, No. 45.
- Elgaaly, M. (1998), "Thin steel plate shear walls behavior and analysis", *Thin Wall. Struct.*, **32**, 152-180.
- FEMA (2000), "Recommended Seismic Design Criteria for New Steel Moment-Frame Buildings", FEMA 350, Prepared by the SAC Joint Venture for FEMA, Washington, D.C.
- Guo, L., Rong, Q., Ma, X. and Zhang, S. (2011), "Behavior of steel plate shear wall connected to frame beams only", *Int. J. Steel Struct.*, **11**(4), 467-479.
- Hoseinzadeh Asl, M. and Safarkhani, M. (2017), "Seismic behavior of steel plate shear wall with reduced boundary beam section", *Thin Wall. Struct.*, **116**, 169-179.
- Jahanpour, A., Moharrami, H. and Aghakoochak, A. (2011), "Evaluation of ultimate capacity of semi-supported steel shear walls", *J. Constr. Steel Res.*, **67**, 1022-1030.
- Kurata, M., Leon, R.T., DesRochesc, R. and Nakashima, M. (2012), "Steel plate shear wall with tension-bracing for seismic rehabilitation of steel frames", *J. Constr. Steel Res.*, **71**, 92-103.
- Nie, J.G., Zhu, L., Fan, J.S. and Mo, Y.L. (2013), "Lateral resistance capacity of stiffened steel plate shear walls", *Thin Wall. Struct.*, **67**, 155-167.
- Pellegrino, C., Maiorana, E. and Modena, C. (2009), "Linear and non-linear behaviour of steel plates with circular and rectangular holes under shear loading", *Thin Wall. Struct.*, **47**, 607-616.
- Purba, R.H. (2006), "Design recommendations for perforated steel plate shear walls", M.Sc. Thesis, Buffalo, N.Y.: State University of New York at Buffalo.
- Purba, R.H. and Bruneau, M. (2015) "Experimental investigation of steel plate shear walls with in-span plastification along horizontal boundary elements", *Eng. Struct.*, **97**, 68-79.
- Roberts, T.M. and Sabouri-Ghomi S. (1992), "Hysteretic characteristics of unstiffened perforated steel plate shear panels", *Thin Wall. Struct.*, **14**, 139-151.
- Sabouri-Ghomi, S., Ventura, M. and Kharrazi, M. (2005), "Shear analysis and design of ductile steel plate walls", *J. Struct. Eng. - ASCE*, **131**(6), 878-889.
- Shekastehband, B., Azaraxsh, A.A. and Showkati, H. (2017), "Experimental and numerical study on seismic behavior of LYS and HYS steel plate shear walls connected to frame beams only", *Arch. Civil Mech. Eng.*, **17**, 154-168.
- Valizadeh, H., Sheidaii, M. and Showkati, H. (2012), "Experimental investigation on cyclic behavior of perforated steel plate shear walls", *J. Constr. Steel Res.*, **70**, 308-316.
- Vatansver, C. and Yardimci, N. (2011), "Experimental investigation of thin steel plate shear walls with different infill-to-boundary frame connections", *Steel Compos. Struct.*, **11**(3), 251-271.
- Vian, D. and Bruneau, M. (2005), "Steel Plate Shear Walls for Seismic Design and Retrofit of Building Structures. Technical Report MCEER-05-0010, MCEER, Buffalo, NY.
- Wei, M.W., Liew, J.Y.R., Yong, D. and Fu, X.U. (2017), "Experimental and numerical investigation of novel partially connected steel plate shear walls", *Thin Wall Struct.*, **132**, 1-15.
- Xue, M. and Lu, L.W. (1994a), "Influence of steel shear wall panels with surrounding frame members", *SSRC annual technical session*, Bethlehem.
- Xue, M. and Lu, L.W. (1994b), "Monotonic and cyclic behavior of infilled steel shear panels", *Proceedings of the 17th Czech and Slovak International Conference on Steel Structures and Bridges*, Bratislava, Slovakia.
- Zirakian, T. and Zhang, J. (2015), "Buckling and yielding behavior of unstiffened slender, moderate, and stocky low yield point steel plates", *Thin Wall. Struct.*, **88**, 105-118.

DL